ATHEROSCLEROSIS AND CALCIUM SIGNALLING IN ENDOTHELIAL CELLS

M. J. Plank, D. J. N. Wall & T. David

Department of Mathematics and Statistics
University of Canterbury
Private Bag 4800
Christchurch, New Zealand

Report Number: UCDMS2004/18 AUG 2004

Atherosclerosis and Calcium Signalling in Endothelial Cells

M. J. Plank, D. J. N. Wall and T. David
University of Canterbury, Private Bag 4800, Christchurch, NZ.

August 18, 2004

Abstract

The link between atherosclerosis and regions of disturbed flow and low wall shear stress is now firmly established, but the causal mechanisms underlying the link are not yet understood. It is now recognised that the endothelium is not simply a passive barrier between the blood and the vessel wall, but plays an active role in maintaining vascular homeostasis and participates in the onset of atherosclerosis. Calcium signalling is one of the principal intracellular signalling mechanisms by which endothelial cells (EC) respond to external stimuli, such as fluid shear stress and ligand binding. Previous studies have separately modelled mass transport of chemical species in the bloodstream and calcium dynamics in EC via the inositol triphosphate (IP_3) signalling pathway. In this study, we integrate these two important components to provide an inclusive model for the calcium response of the endothelium in an arbitrary vessel geometry. This enables the combined effects of fluid flow and biochemical stimulation on EC to be investigated. Model results show that low endothelial calcium levels in the area of disturbed flow at an arterial widening may be one contributing factor to the onset of vascular disease.

1 Introduction

The progressive narrowing and hardening of the arteries, known as atherosclerosis, and associated complications such as thrombosis, heart attack and stroke, are the leading cause of death in the developed world. The pathogenesis of atherosclerosis, in which cholesterol (primarily low density lipoproteins), fibrous substances and inflammatory cells accumulate in the arterial wall has received considerable attention in recent decades (Schachter, 1997).

The disease begins with elevated levels of cholesterol-carrying low density lipoproteins (LDLs) in the layer of the vessel wall known as the intima. This layer is separated from the bloodstream by a monolayer of endothelial cells (EC). In the intima, LDLs are oxidised and induce expression by EC and intimal smooth muscle cells (SMC) of a range of adhesion molecules and chemotactic factors responsible for the adhesion of leukocytes to the endothelium and their subsequent penetration into the intima (Jessup *et al.*, 2004). Additional EC- and SMC-derived chemokines stimulate differentiation of leukocytes into cholesterol-scavenging macrophages, and subsequent macrophage proliferation and expression of LDL receptors. The macrophages engulf LDL and become foam cells, forming a fatty streak in the intima, the characteristic feature of early atherosclerotic lesions (Libby *et al.*, 1997). The accumulation of foam cells in the intima, the first stage of atherosclerosis, is referred to as intimal hyperplasia (IH).

IH is exacerbated by the continued proliferation of SMC in the intima and recruitment of SMC from the sub-intimal layer of the arterial wall known as the media. Activated SMC

synthesise extracellular matrix (ECM) components, such as fibronectin and collagen, which increase the size of lesion and may form a fibrous membrane or 'cap' around the atheroma. Persistent presence of LDLs in the bloodstream allows prolonged growth of the plaque, which may continue for several years. In advanced stages of atheroma, which is now a complex mixture of LDLs, oxidised LDLs, leukocytes, SMC and matrix proteins, macrophages may start to secrete matrix metalloproteases (MMPs) that digest ECM proteins in the plaque and its fibrous cap (Libby, 2003). The plaque may subsequently rupture, often leading to thrombosis and marking the transition from the chronic to the acute, and potentially fatal, stage of atherosclerosis.

There are a variety of well known environmental risk factors, including smoking, high-cholesterol diet and lack of exercise, that increase the likelihood of atherosclerosis. Moreover, it is now established that IH does not occur randomly throughout the circulatory system, but occurs much more frequently near arterial bifurcations and in areas of high vessel curvature (Gimbrone, 1999). IH is strongly associated with disturbed haemodynamic characteristics, such as flow detachment from the arterial wall, flow recirculation and oscillatory flow. IH is particularly well correlated with areas of the vasculature that experience low time-averaged wall shear stress (Malek *et al.*, 1999). The causal link between low wall shear stress and the onset of IH has long been the subject of investigation, but has yet to be fully elucidated.

It has become increasingly recognised that the endothelium is not simply a passive barrier, but plays a crucial role in maintaining vascular homeostasis and regulating the passage of materials between the blood and the vessel wall (Traub and Berk, 1998). EC are sensitive to mechanical stimuli such as wall shear stress, as well as biochemical stimuli such as blood-borne agonists. EC are also a source of numerous vasoactive factors, such as nitric oxide (NO), prostaglandin, endothelin and angiotensin (Schachter, 1997).

In linear sections of the vasculature with steady laminar flow and relatively high wall shear stress (greater than 1 Pa), EC are well aligned in the direction of flow and cell–cell junctions are tight (Gimbrone, 1999). As a consequence, the endothelium is a highly stable cell population, with a very low rates of proliferation and death (Davies, 2000), and low permeability to blood-borne macromolecules, such as LDLs (Schachter, 1997). EC synthesise a number of vasoactive substances, including the potent vasodilators, NO and prostaglandin (Malek *et al.*, 1999). These act in a paracrine manner on SMC in the intima, resulting in relaxation of the arterial wall. Plaque formation in these areas is rare.

In contrast, areas of disturbed flow and low wall shear stress are often associated with a poorly aligned and disorganised endothelium (Davies, 2000). Endothelial turnover and permeability are increased, resulting in enhanced transmission of atherogenic matter into the intima and thus increasing likelihood of IH (Traub and Berk, 1998). Synthesis of NO is reduced, whilst expression of vasoconstrictors and mitogenic factors, such as endothelin and platelet-derived growth factor, are upregulated, increasing the rate of SMC proliferation and protein synthesis in the intima, which accelerates the process of plaque formation (Malek *et al.*, 1999).

The flow characteristics, in addition to determining the shear stress to which the EC are exposed, affect the delivery of blood-borne molecules to the endothelium (Dull and Davies, 1991). These include adenosine nucleotides and thrombin, which are capable of eliciting a response in EC via binding to G-protein-coupled surface receptors. The mechanism by which the EC detect and respond to the prevailing haemodynamic conditions and the delivery of biochemical stimuli is unclear, but is almost certainly linked to intracellular calcium (Ca^{2+}) signalling. Ca^{2+} is a key intracellular second messenger responsible for regulating a variety of cellular functions (Tran *et al.*, 2000).

Under resting conditions, the concentration of free Ca^{2+} in the cytosol is maintained at a very low level by active transport mechanisms that pump Ca^{2+} out of the cell. Ca^{2+} is also pumped into internal storage compartments, primarily the endoplasmic reticulum (ER),

which contain the majority of a quiescent cell's intracellular Ca^{2+} (Alberts *et al.*, 1994). Ca^{2+} signalling can be initiated by the binding of a chemical ligand to cell surface receptors, which causes activation of a G-protein. This leads to intracellular production of the second messenger, inositol triphosphate (IP_3). IP_3 binds to sites on the ER membrane, opening cation channels and thus allowing stored Ca^{2+} to be released into the cytosol (Tran *et al.*, 2000). Depletion of the internal stores appears to stimulate influx of Ca^{2+} into the cell via plasma membrane ion channels (a process known as capacitative Ca^{2+} entry) (Putney *et al.*, 2001), and can also accelerate the rate of release of Ca^{2+} from the ER into the cytosol (Ca^{2+}-induced Ca^{2+} release) (Wood and Gillespie, 1998). Wall shear stress appears to contribute to Ca^{2+} signalling by activating plasma membrane Ca^{2+} channels, thus allowing further influx (Kwan *et al.*, 2003). Wall shear stress may also activate a mechano-sensitive surface receptor linked to the IP_3 signalling pathway, thus increasing the rate of internal Ca^{2+} release (Tseng *et al.*, 1995). Further details of the Ca^{2+} signalling response to biochemical and mechanical stimuli may be found in section 3.

In the cytosol, Ca^{2+} reversibly combines with the protein calmodulin to form a Ca^{2+}–calmodulin complex. This complex activates several intracellular enzymes, including myosin light chain kinase, tyrosine kinase and protein kinase C (which can stimulate entry into the S-phase of the cell cycle via an increase in intracellular hydrogen) (Alberts *et al.*, 1994). The Ca^{2+}–calmodulin complex can also stimulate production of prostaglandin (Jaffe *et al.*, 1987) and activate endothelial NO synthase (eNOS), stimulating production of NO (Lin *et al.*, 2000). As well as being a potent vasodilator, NO inhibits proliferation of smooth muscle cells and aggregation of platelets and is thus a key atheroprotective factor (Shaul, 2003).

In this study, we investigate the link, via endothelial Ca^{2+} signalling, between environmental conditions (applied wall shear stress and delivery of biochemical stimuli) and the onset of IH. The modelling approach has two main components: a fluid dynamical model for the wall shear stress and associated mass transport of blood-borne signalling molecules; and a model for Ca^{2+} signalling within individual EC.

John and Barakat (2001) formulated a model for the mass transport of adenosine triphosphate (ATP) and diphosphate (ADP) in a parallel plate vessel, including the effects of nucleotide uptake and production by EC, and considered both steady and pulsatile flow. David (2003) extended this model to derive an analytical solution for the concentrations of ATP and ADP in an arbitrary vessel geometry with a known shear stress profile. This is particularly important from our point of view as it allows the effects of different vessel geometries, a key factor in the occurrence of atherosclerosis, to be examined. This modelling approach has also been applied to the distribution of platelets in the bloodstream to investigate platelet adhesion and aggregation at the endothelium and consequent thrombus formation (David *et al.*, 2001).

Mathematical models of Ca^{2+} dynamics were first constructed in the context of excitable cells, such as muscle and nerve cells (Meyer and Stryer, 1988; Goldbeter *et al.*, 1990). More recently, Ca^{2+} signalling in EC has also been modelled: Wiesner *et al.* (1996) formulated a comprehensive model of Ca^{2+} dynamics in response to the binding of thrombin to EC surface receptors, which reproduced experimentally observed Ca^{2+} transients. In a subsequent paper, Wiesner *et al.* (1997) studied the effects of wall shear stress on the cell by including shear-sensitive Ca^{2+} channels in the plasma membrane, using a Boltzmann-type law for the fraction of open channels.

Thus the fluid dynamical component and the Ca^{2+} signalling component of the modelling process have been considered separately in previous studies. However, this is, to our knowledge, the first time these components have been coupled, allowing the effects of fluid flow on Ca^{2+} signalling in the endothelium to be directly investigated. We believe this is a key ingredient in an integrated mathematical model of the endothelial response to the full range of physiological stimuli. The fluid mass transport model, based on the work of David (2003),

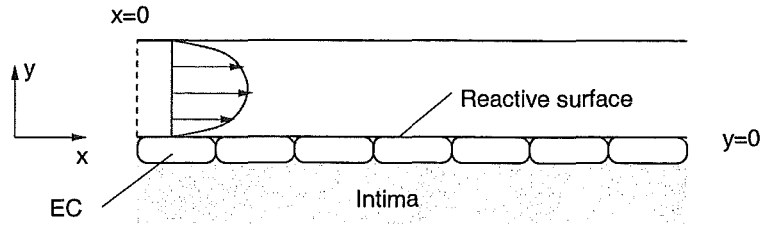

Figure 1: Diagram of the model geometry

is used to calculate the mechanical and biochemical stimuli to which each EC is exposed. The Ca^{2+} model, which is based on the model of Wiesner *et al.* (1997), is then used to study the Ca^{2+} response of each individual EC. The two components are, therefore, only weakly coupled at present; a more general model would allow strong coupling, whereby the Ca^{2+} dynamics have a feedback effect on mass transport by modifying secretion by EC of agonists such as ATP and NO.

The mass transport and Ca^{2+} dynamics models are described in sections 2 and 3 respectively. Results of the Ca^{2+} model for an individual stimulated EC are presented in section 4, whilst the coupling of the two models is addressed in section 5. Finally, the results and their implications are discussed in section 6.

2 Model for Mass Transport

In this section, we describe a model for the mass transport of chemical species in the bloodstream. The model assumes steady flow, but is quite general in the sense that it can be applied to any chemical species with a low diffusion coefficient, and any vessel geometry with a known steady wall shear stress profile (see David (2003) for details).

Figure 1 shows the basic model geometry, which consists of a two-dimensional rigid tube, one side of which (in this case $y = 0$) constitutes a reactive surface, representing a monolayer of endothelial cells (EC). For a given vessel geometry with a known steady flow profile, $(u(x,y), v(x,y))$, with characteristic velocity, u_∞, the concentration, $\phi(x,y)$, of a chemical species with diffusion coefficient D obeys the following advection–diffusion equation in the bulk fluid:

$$u\frac{\partial \phi}{\partial x} + v\frac{\partial \phi}{\partial y} = D\nabla^2\phi. \tag{1}$$

Uptake and production of the species occurs on the reactive surface, $y = 0$, representing the endothelium. We therefore have the following boundary condition on $y = 0$:

$$D\frac{\partial \phi}{\partial y}(x,0) = \frac{V_m \phi(x,0)}{K_m + \phi(x,0)} - S(x). \tag{2}$$

This simulates a Michaelis–Menten reaction for the rate of uptake of the species, and a rate of production, $S(x)$.

The species concentration at the point where medium enters the vessel, $x = x_1$, is a fixed value, ϕ_∞, and the concentration is assumed to approach this value a long way from the endothelium (i.e. as $y \to \infty$):

$$\phi(x_1, y) = \lim_{y\to\infty} \phi(x,y) = \phi_\infty. \tag{3}$$

2.1 Non-Dimensionalisation

We denote the wall shear stress by $\tau_w(x)$ and define the following dimensionless quantities:

$$x' = \frac{x}{L}, \quad y' = \frac{y}{L}, \quad u' = \frac{u}{u_0}, \quad v' = \frac{v}{u_0}, \quad \phi' = \frac{\phi}{\phi_0}, \quad \tau_w' = \frac{\tau_w}{\rho u_0^2}, \quad x_1' = \frac{x_1}{L},$$
$$Re = \frac{u_0 L}{\nu}, \quad Pe = \frac{u_0 L}{D_0}, \quad D' = \frac{D}{D_0}, \quad \phi_\infty' = \frac{\phi_\infty}{\phi_0}, \quad V_m' = \frac{V_m L}{D_0 \phi_0}, \quad K_m' = \frac{K_m}{\phi_0}, \quad u_\infty' = \frac{u_\infty}{u_0},$$
$$S' = \frac{SL}{D_0 \phi_0},$$

where ν and ρ are respectively the kinematic viscosity and density of blood.

An order of magnitude analysis reveals that $\frac{\partial^2 \phi}{\partial y^2} \gg \frac{\partial^2 \phi}{\partial x^2}$, so diffusion in the x-direction may be neglected and the advection–diffusion equation (1), on dropping the dashes, becomes:

$$u\frac{\partial \phi}{\partial x} + v\frac{\partial \phi}{\partial y} = \frac{D}{Pe}\frac{\partial^2 \phi}{\partial y^2}. \tag{4}$$

The boundary conditions (2) and (3) become:

$$D\frac{\partial \phi}{\partial y}(x,0) = \frac{V_m \phi(x,0)}{K_m + \phi(x,0)} - S(x), \tag{5}$$
$$\phi(x_1, y) = \lim_{y\to\infty} \phi(x,y) = \phi_\infty. \tag{6}$$

2.2 Similarity Solution

For many chemical species of interest, such as adenosine nucleotides, the diffusion coefficient, D, in the bloodstream is very low and therefore the Peclet number, Pe, is very high. As a result, the mass transfer boundary layer at the endothelium, $y = 0$, is much thinner than the velocity boundary layer and we may assume that the streamwise velocity, u, is linear with respect to y in the mass transfer layer.

In such cases, it has been shown (David *et al.*, 2001) that if a similarity variable, η, is defined by:

$$\eta = y\frac{(PeRe)^{\frac{1}{3}} |\tau_w(x)|^{\frac{1}{2}}}{\left(9\mathrm{sgn}(x - x_0)\int_{x_0}^{x} |\tau_w(s)|^{\frac{1}{2}}\, ds\right)^{\frac{1}{3}}} \equiv y\beta(x), \tag{7}$$

then the governing equation (4) for chemical concentration may be written as the following ordinary differential equation (ODE):

$$D\frac{d^2\phi}{d\eta^2} + 3\eta^2\frac{d\phi}{d\eta} = 0. \tag{8}$$

The solution of this ODE satisfies

$$\phi(\eta) = A\int_0^\eta \exp\left(-\frac{s^3}{D}\right) ds + \phi(x,0).$$

The boundary condition at the endothelium (5) demands that

$$A = \frac{1}{D\beta(x)}\left(\frac{V_m\phi(x,0)}{K_m + \phi(x,0)} - S(x)\right).$$

Noting that $\phi(\eta) \to AD^{\frac{1}{3}}\frac{\Gamma}{3} + \phi(x,0)$ as $\eta \to \infty$ (where $\frac{\Gamma}{3} = \int_0^\infty e^{-t}t^{-\frac{2}{3}}dt$), the concentration at the endothelium, $\phi(x,0)$, may be found by imposing the boundary condition (6) at $\eta = \infty$.

In the case where the chemical concentration is much smaller than the Michaelis–Menten constant (i.e. $\phi(x,0) \ll K_m$), the full solution may be written:

$$\phi(x,0) = \frac{\phi_\infty \beta(x) D^{\frac{2}{3}} + \frac{\Gamma}{3} S(x)}{\beta(x) D^{\frac{2}{3}} + \frac{\Gamma}{3}\frac{V_m}{K_m}}. \tag{9}$$

The function β defined by (7) has a singularity at $x = 0$. In the case $\tau_w(0) \neq 0$, $\beta(x) \to \infty$ as $x \to 0$, which means that $\lim_{x\to 0} \phi(x,0) = \phi_\infty$. In the case $\tau_w(0) = 0$, Taylor expanding $\tau_w(x)$ about $x = 0$ yields $\lim_{x\to 0} \beta(x) = \left(\frac{PeRe\frac{d\tau_w}{dx}(0)}{6}\right)^{\frac{1}{3}}$.

Notice that, as $x \to \infty$, $\beta(x) \to 0$ and therefore $\phi(x,0) \to \frac{K_m S(x)}{V_m}$. Hence, a long way downstream in a parallel-sided vessel, the species concentration at the endothelium will reach an equilibrium value, with uptake balanced by production. In order to examine the effects of a change in vessel geometry, such as a widening of the artery, we should therefore use this downstream equilibrium value as the *input condition* (ϕ_∞) in equation (9). Thus the species concentration in the region of interest ($x \geq x_1$), where the fluid is assumed to have flowed a long way down a parallel-sided vessel before reaching that region, is given by:

$$\phi(x,0) = \frac{K_m S_\infty}{V_m} \frac{\beta(x) D^{\frac{2}{3}} + \frac{\Gamma}{3}\frac{V_m}{K_m}\frac{S(x)}{S_\infty}}{\beta(x) D^{\frac{2}{3}} + \frac{\Gamma}{3}\frac{V_m}{K_m}}, \tag{10}$$

where $S_\infty = \lim_{x\to x_1} S(x)$ is the "long way downstream" production rate, immediately prior to entering the region of interest.

2.3 Model for ATP

Let us now consider a specific chemical species, adenosine triphosphate (ATP), a ubiquitous signalling molecule present in the blood.

It is known that fluid flow stimulates production of ATP by cultured EC (Milner *et al.*, 1990) and the release rate is thought to increase with the applied wall shear stress (Yamamoto *et al.*, 2003). Following John and Barakat (2001), we consider two possible production rate functions, both of which are increasing functions of wall shear stress, $\tau_w(x)$:

$$S_1(x) = S_0 \frac{\tau_w(x)}{\tau_m}, \quad S_2(x) = S_0 \left(1 - \exp\left(-\frac{\tau_w(x)}{\tau_m}\right)\right)^3, \tag{11}$$

where $S_0, \tau_m \geq 0$ are constants. S_1 a linear function of wall shear stress; S_2 represents a sigmoidal dependence of ATP production of wall shear stress. The parameter values used in the model are shown in Table 1 (for a discussion of these values, see the Appendix).

We now examine the ATP concentration at the endothelium in particular vessel geometries. David (2003) considered a parallel plate geometry and a backward-facing step and imposed a fixed ATP concentration, ϕ_∞, on entry to the vessel at $x = x_1$. However, as discussed above, we use the downstream equilibrium value of $\phi(x,0)$ as the input condition. For the parallel plate setup, the wall shear stress is uniform, so $S(x) \equiv S_\infty$ and, using the equilibrium input condition, equation (10) shows that $\phi(x,0)$ is independent of x. This is unsurprising since the species concentration has already reached equilibrium by the time it reaches $x = x_1$ and there is no inhomogeneity to disturb it from this equilibrium.

However, for the backward-facing step (see Figure 2), representing a widening of the vessel, differences in wall shear stress along the vessel wall will cause variations in the species concentration. We therefore focus on the backward-facing step as a simple model geometry in

Dimensional values	
Bulk ATP concentration	$\phi_\infty = 0.1\ \mu$M
ATP uptake rate	$V_m = 8 \times 10^{-3}\ \mu$M m s^{-1}
ATP Michaelis–Menten constant	$K_m = 475\ \mu$M
ATP diffusion coefficient	$D = 2.36 \times 10^{-10}$ m^{2}s^{-1}
Maximum ATP production rate	$S_0 = 10^{-6}\ \mu$M m s^{-1}
Characteristic WSS for ATP production	$\tau_m = 1$ kg m^{-1} s^{-2}
Step height	$h = 2.5 \times 10^{-4}$ m
Reference lengthscale	$L = 2.5 \times 10^{-4}$ m
Reference ATP concentration	$\phi_0 = 0.1\ \mu$M
Reference velocity	$u_0 = 1.04 \times 10^{-2}$ m s^{-1}
Reference diffusion coefficient	$D_0 = 2.36 \times 10^{-10}$ m^{2}s^{-1}
Kinematic viscosity of blood	$\nu = 4 \times 10^{-6}$ m^{2}s^{-1}
Density of blood	$\rho = 1000$ kg m^{-3}
Dimensionless values	
Reynolds number	$Re = 0.651$
Peclet number	$Pe = 1.10 \times 10^4$
Bulk ATP concentration	$\phi_\infty = 1$
ATP uptake rate	$V_m = 84700$
ATP diffusion coefficient	$D = 1$
Maximum ATP production rate	$S_0 = 10.6$
Characteristic WSS for ATP production	$\tau_m = 9.22$
ATP Michaelis–Menten constant	$K_m = 4750$

Table 1: Parameter values used in the model for mass transport.

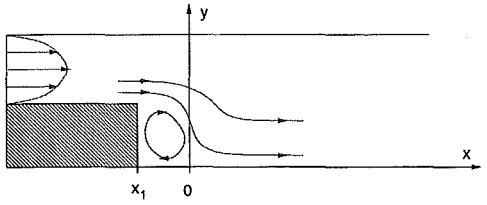

Figure 2: Diagram of the backward-facing step geometry, representing a widening of the artery. The flow detaches from the endothelium at $x = x_1$ and reattaches at $x = x_0 = 0$.

which flow detachment and recirculation occur. The flow detaches from the endothelium at the entry point $x = x_1$, the reattachment point is at $x = x_0 = 0$ and there is a recirculation zone for $x_1 < x < x_0$. The wall shear stress (as calculated in David (2003)) and ATP concentration (as given by (10)) for the backward-facing step are shown in Figure 3 for two different characteristic flow velocities, u_∞. The sigmoidal ATP production function (S_2) is used. Note that the lower the flow velocity, the lower the shear stress and the smaller the recirculation zone. ATP concentration is lowest in areas of low wall shear stress, particularly at the backward-edge of the recirculation zone. This is because ATP production is low in these areas and because the low flow velocity allows more ATP to enter the mass transfer layer and be consumed by the EC. Results (not shown) using the linear ATP production function (S_1) with $\tau_m = 46.1$ are very similar and, from now on, we will use S_2 in the simulations as the rate-limiting property of this function makes it more realistic than S_1.

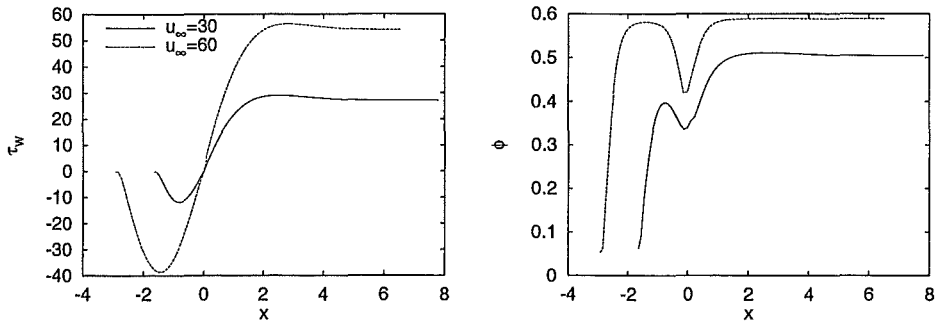

Figure 3: Graph of wall shear stress and ATP concentration against x in the backward-facing step for flow velocities $u_\infty = 30$ and $u_\infty = 60$: (a) Wall shear stress, $\tau_w(x)$. (b) ATP concentration at the endothelium, $\phi(x, 0)$. The origin ($x = 0$) is taken to be at the reattachment point (where $\tau_w = 0$).

3 Model for Endothelial Calcium Dynamics

Calcium (Ca^{2+}) is a key intracellular second messenger in almost all eukaryotic cells. EC are no exception and intracellular Ca^{2+} serves as a positive or negative regulatory signal for a range of cell functions, including: secretion of vasoactive agents (such as NO and prostaglandin), adhesion molecules and growth factors and inhibitors; cell alignment in the direction of blood flow; and cell proliferation and apoptosis (Schilling and Elliott, 1992; Tran *et al.*, 2000). Under resting conditions, the majority of an EC's Ca^{2+} is stored in internal compartments, mainly the endoplasmic reticulum (ER), and the concentration of free Ca^{2+} in the cytosol is very low. Transduction of an external biochemical or mechanical signal, however, stimulates both a release of Ca^{2+} from internal stores and an influx of Ca^{2+} across the plasma membrane (Alberts *et al.*, 1994). This can result in a single transient peak of cytosolic Ca^{2+} concentration, followed by a return towards baseline, or in sustained Ca^{2+} oscillations (Dull and Davies, 1991; Shen *et al.*, 1992). The decay in cytosolic Ca^{2+} following internal Ca^{2+} release is a result of the plasma membrane Ca^{2+}-ATPase, which pumps Ca^{2+} from the cytosol out of the cell, and the ER Ca^{2+}-ATPase, which resequesters Ca^{2+} from the cytosol back into the ER (Schilling and Elliott, 1992).

The endothelium is a complex signalling barrier that is sensitive to a variety of external stimuli. Here we focus on two key external stimuli: the activation of cell surface receptors by ligand and wall shear stress.

The first of these is a biochemical stimulus and we use ATP as a generic model ligand for EC surface receptors. The binding of ATP to G-protein-coupled receptors on the EC surface initiates a signal transduction cascade involving activation of phospholipase C and cleavage of phosphatidylinositol biphosphate (PIP_2) to form inositol triphosphate (IP_3) (Alberts *et al.*, 1994). IP_3 is a key intracellular second messenger which opens Ca^{2+} channels on the ER, thus releasing Ca^{2+} into the cytosol (Tran *et al.*, 2000). This internal Ca^{2+} release may trigger a positive feedback mechanism, whereby more channels are opened, accelerating the rate of Ca^{2+} release. This phenomenon is termed Ca^{2+}-induced Ca^{2+} release (CICR) (Wood and Gillespie, 1998). The increased concentration of cytosolic Ca^{2+} can also act cooperatively to increase IP_3 production, via increased phospholipase C activity (Mahama and Linderman, 1994; Meyer and Stryer, 1988). Furthermore, release of Ca^{2+} from stores appears to stimulates influx of Ca^{2+} across the plasma membrane, a process termed capacitative calcium entry (CCE) (Putney *et al.*, 2001). The mechanism of action of CCE is unclear and a variety

of explanations have been suggested, including: direct regulation of Ca^{2+} channels in the plasma membrane by Ca^{2+} concentration in the cytosol; release-sensitive production of a diffusible "calcium influx factor"; activation of Ca^{2+} channels by kinases (such as tyrosine kinase and myosin light chain kinase), produced as a result of Ca^{2+}–calmodulin complexes in the cytosol; conformational coupling between the IP_3 sensitive channel in the ER and Ca^{2+} channels in the plasma membrane (Watanabe *et al.*, 1998; Tran *et al.*, 2000; Putney *et al.*, 2001). CCE appears to be inhibited by cyclic guanosine monophosphate (cGMP) and G-kinase, which are produced as downstream effects of NO and Ca^{2+} signalling. This raises the possibility of a negative feedback mechanism for Ca^{2+} influx, preventing the cytosolic Ca^{2+} concentration from becoming too high (Kwan *et al.*, 2000).

The second stimulus to be considered, wall shear stress, is a mechanical one. It is well known that the physical forces exerted on EC by fluid flow result in an internal signalling response (Geiger *et al.*, 1992; Tseng *et al.*, 1995). The mechanism whereby the cell detects and responds to the mechanical stimulus is unclear, but there are two (not mutually exclusive) possibilities that have gained some biological evidence. One is the existence of Ca^{2+} channels in the plasma membrane that are directly gated by shear stress (Kwan *et al.*, 2003); the second is a shear-sensitive mechano-receptor that is linked to the IP_3 signalling pathway (Tseng *et al.*, 1995). However, very few data exist regarding mechano-transduction via IP_3 in EC, so we focus on the first of these mechanisms.

Thus the key processes incorporated in the model of Ca^{2+} dynamics are as follows (see Figure 4 for a diagrammatic representation):

1. Binding of ATP into surface receptors reversibly forms a receptor–ligand complex, which then decomposes to a free receptor (which is recycled back to the cell surface) and some product. This decomposition stimulates internal production of IP_3. Note that this is a bundled step, including several processes such as the activation of a G-protein and phospholipase C and the cleavage of PIP_2.
2. IP_3 opens Ca^{2+} channels in the ER, so the rate of internal Ca^{2+} release is an increasing function of IP_3 concentration.
3. Both the rate of IP_3 production and the rate of internal Ca^{2+} release can be enhanced by cytosolic free Ca^{2+}. This is part of the CICR mechanism.
4. The rate of Ca^{2+} influx due to CCE is an increasing function of the degree of depletion of the ER below resting levels, as well as the Ca^{2+} concentration difference across the plasma membrane (i.e. the difference between the external and cytosolic concentrations). This is a generic mechanism for CCE because details of the intermediate steps by which depletion of internal stores stimulates Ca^{2+} influx are unknown.
5. The rate of Ca^{2+} influx through shear-gated channels is an increasing function of the wall shear stress to which the EC is exposed.
6. Wall shear stress can also increases IP_3 production via a shear-sensitive receptor.
7. Cytosolic Ca^{2+} is resequestered back into the ER by a Ca^{2+}-ATPase and is pumped out of the cell by a plasma membrane Ca^{2+}-ATPase and Ca^{2+}-Na^{+} exchanger.
8. Cytosolic Ca^{2+} is reversibly buffered to proteins such as calmodulin.

We now construct a mathematical model of these processes, which is based on the model of Wiesner *et al.* (1996). The four quantities we model are the concentrations of IP_3 in the cytosol (i), free Ca^{2+} in the cytosol (Ca_c), buffered Ca^{2+} in the cytosol (Ca_b) and Ca^{2+} in the internal stores (Ca_s). The model is a non-spatial, ODE-type model and effectively assumes that these concentrations, and the external stimuli to which they are sensitive, are

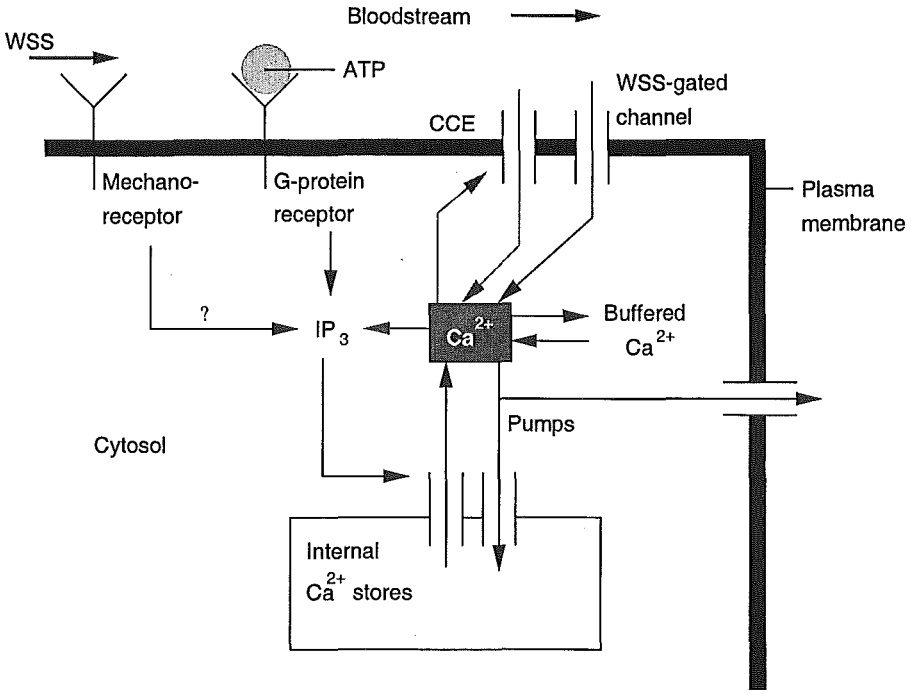

Figure 4: Diagram of the key Ca^{2+} processes included in the mathematical model. Receptor activation stimulates IP_3 generation which releases Ca^{2+} from internal stores into the cytosol. This can have a positive feedback effect by increasing the rate of IP_3 production and the rate of Ca^{2+} release (CICR). Depletion of internal stores also stimulates Ca^{2+} influx (CCE). Wall shear stress can increase Ca^{2+} influx via shear-gated Ca^{2+} channels. Wall shear stress may also contribute to IP_3 signalling via a shear-sensitive receptor. Cytosolic Ca^{2+} is reversibly buffered by proteins, is resequestered back into the internal stores and is pumped across the plasma membrane out of the cell.

uniform across the cell. This is a reasonable first approximation because the size of the cell is small (the average axial length of an EC is between 10^{-5} and 10^{-4} m) compared to the length of the vessel being examined (which is of the order 10^{-3} m). Our model will therefore be an initial value problem, taking the form of three ODEs with associated initial conditions.

We begin with the IP_3 equation, which consists simply of a term for production of IP_3 and natural decay of IP_3 with rate constant $k_2 \geq 0$. As mentioned above, we bundle the G-protein-coupled transduction cascade into a single simplified reaction. In this reaction, one molecule of ligand, ATP (A), combines reversibly with one free receptor (R_A) to form a receptor–ligand complex (AR_A). This complex decomposes into a modified receptor, R'_A (which is recycled back to the cell surface to become R_A) and activates a sequence of steps which culminates in the production of n molecules of IP_3 (I). This may be written:

$$A + R_A \underset{k_s}{\overset{k_r}{\rightleftharpoons}} AR_A \xrightarrow{k_d} R'_A + nI, \tag{12}$$

For reactions of this type, where the concentration of the intermediate complex, AR_A is in pseudo-steady state, the Michaelis–Menten law applies (for details see Murray (1993), ch. 5), and the rate of change of the product, I, is:

$$\frac{d}{dt}[I](t) = \frac{k_1 [A](t)}{K_c + [A](t)},$$

where $[X]$ denotes the concentration of substance X, $k_1 = k_d n [AR_A](0)$ and $K_c = \frac{k_s + k_d}{k_r}$.

In the case of IP_3 generation in EC, we assume, as discussed above, that the production rate k_1 is an increasing function of Ca_c. We use a saturating function of the Michaelis–Menten type: $k_1(Ca_c) = k_1 \frac{Ca_c}{K_1 + Ca_c}$ for constants, $k_1, K_1 \geq 0$ (Mahama and Linderman, 1994). We hence have the following ODE for intracellular IP_3 concentration (i):

$$\frac{di}{dt} = k_1 \frac{\phi}{K_c + \phi} \frac{Ca_c}{K_1 + Ca_c} - k_2 i. \tag{13}$$

where ϕ is the concentration of ATP at the cell surface.

Transfer of Ca^{2+} between the ER and the cytosol consists of two ionic fluxes: the rate of release of Ca^{2+} from the ER, q_{rel}, and the rate of resequestration of Ca^{2+} back into the ER, q_{res}. There are four additional fluxes that contribute to the free cytosolic Ca^{2+}: the rate of influx, q_{in}, the rate of efflux, q_{out}, and the 'on' and 'off' rates of cytosolic buffering, q_{on} and q_{off}. Allowing for the ratio of the volume of the cytosol to the volume of the ER (V_r), we have the following ODEs for the free, buffered and stored Ca^{2+} concentrations:

$$\frac{dCa_c}{dt} = q_{\text{rel}} - q_{\text{res}} + q_{\text{in}} - q_{\text{out}} - q_{\text{on}} + q_{\text{off}}, \tag{14}$$

$$\frac{dCa_b}{dt} = q_{\text{on}} - q_{\text{off}}, \tag{15}$$

$$\frac{dCa_s}{dt} = -V_r (q_{\text{rel}} - q_{\text{res}}). \tag{16}$$

We now give functional forms for each of these fluxes. Following Meyer and Stryer (1988), we take the release flux, q_{rel}, to be saturably dependent on IP_3, with a cubic exponent, reflecting the fact that three IP_3 molecules must be bound to an ER Ca^{2+} channel in order to open it. To represent CICR, we take the release rate to be saturably dependent on Ca_c and linearly dependent on Ca_s:

$$q_{\text{rel}} = k_3 \frac{Ca_c}{K_{\text{CICR}} + Ca_c} \left(\frac{i}{K_2 + i}\right)^3 Ca_s,$$

for constants $k_3, K_{\text{CICR}}, K_2 \geq 0$.

Meyer and Stryer (1988) give a net resequestration flux of:

$$q_{\text{res}} = k_4 \left(\frac{Ca_c}{K_3 + Ca_c} \right)^2 - k_5 Ca_s^2,$$

for constants $k_4, k_5, K_3 \geq 0$. The resequestration rate is squared because the ER Ca^{2+}-ATPase transports two calcium ions from the cytosol into the ER per cycle.

Ca^{2+} influx is assumed to be composed of CCE and a wall shear stress-dependent influx. We take the CCE rate to be proportional to the degree of depletion of the ER below its resting level, $Ca_{s,0}$, and the concentration difference across the plasma membrane, $Ca_{\text{ex}} - Ca_s$, where Ca_{ex} is the (assumed constant) external concentration of Ca^{2+}. Note that Ca_{ex} is actually the concentration in the bloodstream, which should be coupled to the mass transport model via the Ca^{2+} influx and efflux terms. However, the concentration in the bloodstream is very large compared to the cytosolic concentration, so the effects of Ca^{2+} ionic exchange across the plasma membrane will be negligible and the assumption of constant concentration is reasonable.

Following Wiesner *et al.* (1997), we take the shear-dependent influx to be proportional to the fraction of open Ca^{2+} channels in the plasma membrane, which has a Boltzmann dependence on the strain energy density in the plasma membrane, $W(\tau_w)$. This gives a sigmoidal relationship between shear-dependent influx and the applied wall shear stress. We therefore have the following expression for Ca^{2+} influx:

$$q_{\text{in}} = k_{\text{CCE}} \left(Ca_{s,0} - Ca_s \right) \left(Ca_{\text{ex}} - Ca_c \right) + \frac{q_{\max}}{1 + \alpha \exp\left(-W(\tau_w) \right)},$$

where $k_{\text{CCE}}, q_{\max}, \alpha \geq 0$ are constants. $(1+\alpha)^{-1}$ is the probability that a channel is in the open state in the no-load case ($W = 0$).

The function, W, of the applied wall shear stress, τ_w, was given by Wiesner *et al.* (1997) as:

$$W(\tau_w) = \frac{f_e \left(\epsilon \tau_w l + \sqrt{16\delta^2 + \epsilon^2 \tau_w^2 l^2} - 4\delta \right)^2}{8kT_e N \left(\epsilon \tau_w l + \sqrt{16\delta^2 + \epsilon^2 \tau_w^2 l^2} \right)}.$$

$0 \leq \epsilon \leq 1$ is the fraction of the applied load borne by the plasma membrane; the remaining fraction is borne by other parts of the cell, primarily the cytoskeleton. $0 \leq f_e \leq 1$ is the fraction of the energy within the membrane that gates the shear-sensitive Ca^{2+} channels. $l > 0$ is the length of the cell in the direction of flow, $\delta \geq 0$ is the membrane shear modulus, $T_e \geq 0$ is the temperature, $N \geq 0$ is the ion channel density per unit area and k is the Boltzmann constant.

Valant *et al.* (1992) gave the rate of Ca^{2+} extrusion as a sum of Hill functions. In order to avoid over-complicating the model whilst retaining the key behavioural elements, we approximate this efflux rate as a single Michaelis–Menten term, which is close to the rate of Valant *et al.* (1992) in the physiological concentration range. We therefore take:

$$q_{\text{out}} = \frac{k_8 Ca_c}{K_4 + Ca_c},$$

where $k_8, K_4 \geq 0$ are constants. This efflux rate incorporates Ca^{2+} extrusion via the plasma membrane Ca^{2+}-ATPase and Ca^{2+}-Na^+ exchanger.

Finally, we follow Jafri *et al.* (1992) and take the following buffering rates:

$$\begin{aligned} q_{\text{on}} &= k_6 Ca_c \left(B_T - Ca_b \right), \\ q_{\text{off}} &= k_7 Ca_b, \end{aligned}$$

where Ca_b is the concentration of cytosolic Ca^{2+} that is complexed to buffering proteins. $k_6, k_7 \geq 0$ are the buffering and debuffering rate constants respectively and $B_T \geq 0$ is the total concentration of Ca^{2+} buffering sites on proteins in the cytosol.

However, these buffering reactions take place on a faster timescale than the influx, efflux and exchange dynamics described above. We may therefore assume that the buffering reaction is in pseudo-steady state. From now on, we consider only the total cytosolic Ca^{2+} concentration, $Ca_t = Ca_c + Ca_b$ and, on setting $q_{\text{on}} + q_{\text{off}} = 0$, obtain the relationship:

$$2Ca_c = Ca_t - B_T - \frac{k_7}{k_6} + \left(\left(Ca_t - B_T - \frac{k_7}{k_6}\right)^2 + 4\frac{k_7}{k_6}Ca_t\right)^{\frac{1}{2}},$$

which is obtained by setting $\frac{dCa_b}{dt} = 0$.

Summing equations (14) and (15) and substituting the above expressions for the fluxes into the resulting equation and into equation (16) gives the following ODEs:

$$\begin{aligned}\frac{dCa_t}{dt} &= k_3\frac{Ca_c}{K_{\text{CICR}} + Ca_c}\left(\frac{i}{K_2 + i}\right)^3 Ca_s - k_4\left(\frac{Ca_c}{K_3 + Ca_c}\right)^2 + k_5 Ca_s^2 \qquad (17)\\ &\quad + k_{\text{CCE}}\left(Ca_{s,0} - Ca_s\right)\left(Ca_{\text{ex}} - Ca_c\right) + \frac{q_{\max}}{1 + \alpha\exp\left(-f_e W\left(\tau_w\right)\right)} - \frac{k_8 Ca_c}{K_4 + Ca_c},\\ \frac{dCa_s}{dt} &= -V_r\left(k_3\frac{Ca_c}{K_{\text{CICR}} + Ca_c}\left(\frac{i}{K_2 + i}\right)^3 Ca_s - k_4\left(\frac{Ca_c}{K_3 + Ca_c}\right)^2 + k_5 Ca_s^2\right). \qquad (18)\end{aligned}$$

Under resting conditions, there is no IP_3, and the free Ca^{2+} in the cytosol and the Ca^{2+} in the internal stores are at resting concentration, Ca_0, and $Ca_{s,0}$ respectively. We hence take the following initial conditions:

$$\begin{aligned} i\left(0\right) &= 0, \qquad (19)\\ Ca_t\left(0\right) &= Ca_0\frac{Ca_0 + B_T + \frac{k_7}{k_6}}{Ca_0 + \frac{k_7}{k_6}}, \qquad (20)\\ Ca_s\left(0\right) &= Ca_{s,0}. \qquad (21)\end{aligned}$$

3.1 Non-Dimensionalisation

Let

$$\begin{array}{llllll} i' = \frac{i}{K_4}, & Ca_t' = \frac{Ca_t}{K_4}, & Ca_c' = \frac{Ca_c}{K_4}, & Ca_s' = \frac{Ca_s}{K_4}, & \phi' = \frac{\phi}{\phi_0}, & \tau_w' = \frac{\tau_w}{\rho u_0^2},\\ K_{\text{CICR}}' = \frac{K_{\text{CICR}}}{K_4}, & k_1' = \frac{k_1 T}{K_4}, & k_2' = k_2 T, & k_3' = k_3 T, & k_4' = \frac{k_4 T}{K_4}, & k_5' = k_5 T K_4,\\ k_{\text{CCE}}' = k_{\text{CCE}} K_4 T, & K_c' = \frac{K_c}{\phi_0}, & K_1' = \frac{K_1}{K_4}, & K_2' = \frac{K_2}{K_4}, & K_3' = \frac{K_3}{K_4}, & t' = \frac{t}{T},\\ Ca_{s,0}' = \frac{Ca_{s,0}}{K_4}, & Ca_{\text{ex}}' = \frac{Ca_{\text{ex}}}{K_4}, & Ca_0' = \frac{Ca_0}{K_4}, & q_{\max}' = \frac{q_{\max} T}{K_4}, & k_8' = \frac{k_8 T}{K_4}, & k_b' = \frac{k_7}{k_6 K_4},\\ B_T' = \frac{B_T}{K_4}, & \delta' = \frac{\delta}{\rho u_0^2 l}, & W_0 = \frac{\rho u_0^2 l}{8kT_e N}, & & & \end{array}$$

where T is a characteristic timescale (we take $T = 500$ s, which is the value used by Wiesner *et al.* (1996)).

On dropping the dashes, the three ODEs (13), (17) and (18) become:

$$\begin{aligned}\frac{di}{dt} &= k_1\frac{\phi}{K_c + \phi}\frac{Ca_c}{K_1 + Ca_c} - k_2 i \qquad (22)\\ \frac{dCa_t}{dt} &= k_3\frac{Ca_c}{K_{\text{CICR}} + Ca_c}\left(\frac{i}{K_2 + i}\right)^3 Ca_s - k_4\left(\frac{Ca_c}{K_3 + Ca_c}\right)^2 + k_5 Ca_s^2 \qquad (23)\end{aligned}$$

$$+k_{\mathrm{CCE}}\left(Ca_{s,0}-Ca_s\right)\left(Ca_{\mathrm{ex}}-Ca_c\right)+\frac{q_{\max}}{1+\alpha\exp\left(-W\left(\tau_w\right)\right)}-\frac{k_8Ca_c}{1+Ca_c},$$

$$\frac{dCa_s}{dt} = -V_r\left(k_3\frac{Ca_c}{K_{\mathrm{CICR}}+Ca_c}\left(\frac{i}{K_2+i}\right)^3Ca_s-k_4\left(\frac{Ca_c}{K_3+Ca_c}\right)^2+k_5Ca_s^2\right), \quad (24)$$

where

$$W\left(\tau_w\right)=f_eW_0\frac{\left(\epsilon\tau_w+\sqrt{16\delta^2+\epsilon^2\tau_w^2}-4\delta\right)^2}{\epsilon\tau_w+\sqrt{16\delta^2+\epsilon^2\tau_w^2}}.$$

The free cytosolic Ca^{2+} concentration is given by:

$$2Ca_c=Ca_t-B_T-k_b+\left(\left(Ca_t-B_T-k_b\right)^2+4k_bCa_t\right)^{\frac{1}{2}}.$$

Finally, the initial conditions (19)–(21) become

$$i\left(0\right) = 0, \quad (25)$$

$$Ca_t\left(0\right) = Ca_0\frac{Ca_0+B_T+k_b}{Ca_0+k_b}, \quad (26)$$

$$Ca_s\left(0\right) = Ca_{s,0}. \quad (27)$$

The parameter values used in the model are shown in Table 2 (for a discussion of these values, see the Appendix). Extensive numerical analysis has revealed that the model is structurally stable with respect to changes in parameter values.

4 Single Cell Results

Numerical simulations of the Ca^{2+} dynamics model described in section 3 were run. The ODEs (22)–(24) were solved using an adaptive step Runge–Kutta routine, with external ATP concentration, $\phi = 0.9$, and wall shear stress, $\tau_w = 9.2$. The system thus represents a single cell stimulated with a step increase in the external ATP concentration and in the applied wall shear stress.

Figure 5 shows time courses for the IP_3 and free cytosolic and stored Ca^{2+} concentrations. Receptor activation by ATP stimulates production of IP_3, which rapidly reaches a steady level. This stimulates release of Ca^{2+} from stores, resulting in a transient increase in the cytosolic Ca^{2+}, and a corresponding decrease in stored Ca^{2+}. Subsequently, cytosolic Ca^{2+} gradually decays to a plateau value as Ca^{2+} is pumped out of the cell via the plasma membrane Ca^{2+}-ATPase. The plateau value is slightly higher than the resting level because of the sustained presence of IP_3 and because of store-operated Ca^{2+} influx (CCE). If the external ATP and shear stress stimuli are removed (i.e. $\phi = 0$ and $\tau_w = 0$ for $t > t_c$), IP_3 production ceases and IP_3 rapidly decays. The cytosolic Ca^{2+} concentration quickly returns to baseline and the internal stores recover towards their resting concentration. The finding of a cytosolic Ca^{2+} transient is in agreement with experimental data (Dull and Davies, 1991; Yamamoto *et al.*, 2000) and previous mathematical modelling results (Wiesner *et al.*, 1996), and the model reproduces realistic response times and peak Ca^{2+} concentrations.

It has been reported (Dull and Davies, 1991; Shen *et al.*, 1992) that, under certain conditions, endothelial cells can exhibit sustained or transient Ca^{2+} oscillations. The mathematical model is also capable of supporting such oscillations. For example, Figure 6 shows a simulation with $k_1 = 35.8$, $k_4 = 7.81 \times 10^4$, $k_5 = 1.6 \times 10^{-4}$ and $K_1 = 1$. These parameter

Dimensional values	
IP_3 production rate	$k_1 = 5.46 \times 10^{-3}$ μM s^{-1}
IP_3 decay rate	$k_2 = 0.2$ s^{-1}
Ca^{2+} release rate	$k_3 = 6.64$ s^{-1}
Ca^{2+} resequestration rate	$k_4 = 5$ μM s^{-1}
Ca^{2+} leak rate	$k_5 = 10^{-7}$ μM^{-1} s^{-1}
Ca^{2+} buffering rate	$k_6 = 100$ μM^{-1} s^{-1}
Ca^{2+} debuffering rate	$k_7 = 300$ s^{-1}
Ca^{2+} efflux rate	$k_8 = 24.7$ μM s^{-1}
Max. WSS-induced Ca^{2+} influx rate	$q_{\max} = 17.6$ μM s^{-1}
CCE rate	$k_{\text{CCE}} = 8 \times 10^{-7}$ μM^{-1} s^{-1}
Resting cytosolic Ca^{2+} concentration	$Ca_0 = 0.1$ μM
Resting stored Ca^{2+} concentration	$Ca_{s,0} = 2828$ μM
External Ca^{2+} concentration	$Ca_{\text{ex}} = 1500$ μM
Concentration of Ca^{2+} buffering sites	$B_T = 120$ μM
Michaelis–Menten constants	$K_{\text{CICR}} = 0$ μM
	$K_1 = 0$ μM
	$K_2 = 0.2$ μM
	$K_3 = 0.15$ μM
	$K_4 = 0.32$ μM
	$K_c = 0.026$ μM
Membrane shear modulus	$\delta = 10^{-5}$ kg s^{-2}
Cell length in direction of flow	$l = 3.5 \times 10^{-5}$ m
Temperature	$T_e = 310$ K
Ca^{2+} channel area density	$N = 10^{12}$ m^{-2}
Boltzmann constant	$k = 1.3807 \times 10^{-23}$ kg m^2 s^{-2} K^{-1}
Reference timescale	$T = 500$ s
Dimensionless values	
IP_3 production rate	$k_1 = 8.53$
IP_3 decay rate	$k_2 = 100$
Ca^{2+} release rate	$k_3 = 3320$
Ca^{2+} resequestration rate	$k_4 = 7810$
Ca^{2+} leak rate	$k_5 = 1.6 \times 10^{-5}$
Ca^{2+} efflux rate	$k_8 = 38600$
Max. WSS-induced Ca^{2+} influx rate	$q_{\max} = 27500$
CCE rate	$k_{\text{CCE}} = 1.28 \times 10^{-4}$
Ratio of Ca^{2+} buffering rates	$k_b = 9.38$
Resting cytosolic Ca^{2+} concentration	$Ca_0 = 0.313$
Resting stored Ca^{2+} concentration	$Ca_{s,0} = 8840$
External Ca^{2+} concentration	$Ca_{\text{ex}} = 4690$
Concentration of Ca^{2+} buffering sites	$B_T = 375$
Michaelis–Menten constants	$K_1 = 0$
	$K_2 = 0.625$
	$K_3 = 0.469$
	$K_c = 0.26$
Ratio of cytosolic and ER volumes	$V_r = 3.5$
Membrane shear modulus	$\delta = 2.63$
Strain energy density constant	$W_0 = 111$
Plasma membrane load fraction	$\epsilon = 0.1$
Plasma membrane energy gating fraction	$f_e = 0.0134$
No-load channel constant	$\alpha = 2$

Table 2: Parameter values used in the model for calcium dynamics.

values represent an increased rate of IP_3 production and faster exchange of Ca^{2+} between the internal stores and the cytosol. In addition, taking K_1 to be non-zero activates the positive feedback mechanism for internal Ca^{2+} release: free cytosolic Ca^{2+} acts cooperatively with receptor activation to increase IP_3 production. The result of this is sustained oscillations in the concentrations of IP_3 and cytosolic and stored Ca^{2+}.

In order to assess the potential physiological significance of Ca^{2+} oscillations, we now conduct a numerical bifurcation analysis of the model. Using the above parameter values, we examine the behaviour of the system for a range of values of the external ATP concentration, ϕ. This will reveal which strengths of biochemical stimulation result in Ca^{2+} oscillations and the characteristics of the transition between the non-oscillatory and oscillatory regimes.

Figure 7(a) shows a bifurcation diagram, plotting the norm of the steady solutions of the system, whether they are fixed points (i.e. non-oscillating) or periodic orbits (i.e. oscillating), against ϕ, for fixed wall shear stress. The ATP concentration in the bloodstream is not known exactly, but is thought to be less than 2 μM (Yamamoto *et al.*, 2000) (which is equivalent to a dimensionless value of 20), so Figure 7(a) shows behaviour for ATP concentration in the physiological range. For $\phi < 0.42$, there is a single, stable fixed point, indicating that the system eventually settles down to a steady state (this corresponds to the plateau phase in a stimulated cell). For $0.42 < \phi < 9.38$, the fixed point is unstable, and there is a stable periodic orbit, indicating that the system undergoes sustained Ca^{2+} oscillations. The two regimes are separated by a super-critical Hopf bifurcation, which means that the stable oscillations bifurcate smoothly from the fixed point. Physiologically, this means that as the ATP concentration is increased past the bifurcation point, oscillations begin at small amplitude, and then gradually increase: there is no sudden appearance of oscillatory behaviour. For $9.38 < \phi$, the fixed point becomes stable once again via a second super-critical Hopf bifurcation. Hence as the ATP concentration increases to very high values, the oscillations gradually diminish in amplitude and eventually disappear.

Holding the ATP concentration fixed and varying the applied wall shear stress, τ_w, gives similar results (see Figure 7(b)). For low and very high wall shear stress, the system evolves to a stable fixed point; for intermediate values of wall shear stress, Ca^{2+} oscillations occur.

5 Coupling of the Models for Mass Transport and Calcium Dynamics

We now conduct simulations of the Ca^{2+} dynamics over a length of a blood vessel consisting of a finite number of EC. Taking a given vessel geometry with known steady flow and shear stress profiles, we use the mass transport model described in section 2 to calculate the wall shear stress, τ_w, and ATP concentration, ϕ, to which each EC is exposed. We then use the Ca^{2+} dynamics model described in section 3 to examine the response of each cell. This will allow us to analyse differences in the Ca^{2+} signalling process in different areas of the vessel.

We begin with the original (non-oscillatory) parameter regime (see Table 2). Figure 8 shows how the steady (plateau) concentration of cytosolic Ca^{2+} varies along the vessel in a backward-facing step for two different characteristic flow velocities, u_∞ (the corresponding shear stress and ATP profiles are those shown in Figure 3). In both cases, Ca^{2+} is lowest in EC in the recirculation zone ($x_1 \leq x < 0$) and this is because both the wall shear stress and ATP concentration are low in this area (see Figure 3). In particular, the lowest Ca^{2+} concentration occurs at the backward edge of the recirculation zone ($x = x_1$), where both the magnitude of the wall shear stress and the concentration of ATP attain their minimum values. The variation in Ca^{2+} levels is most marked for higher velocities because high velocity causes a greater range of wall shear stress along the vessel.

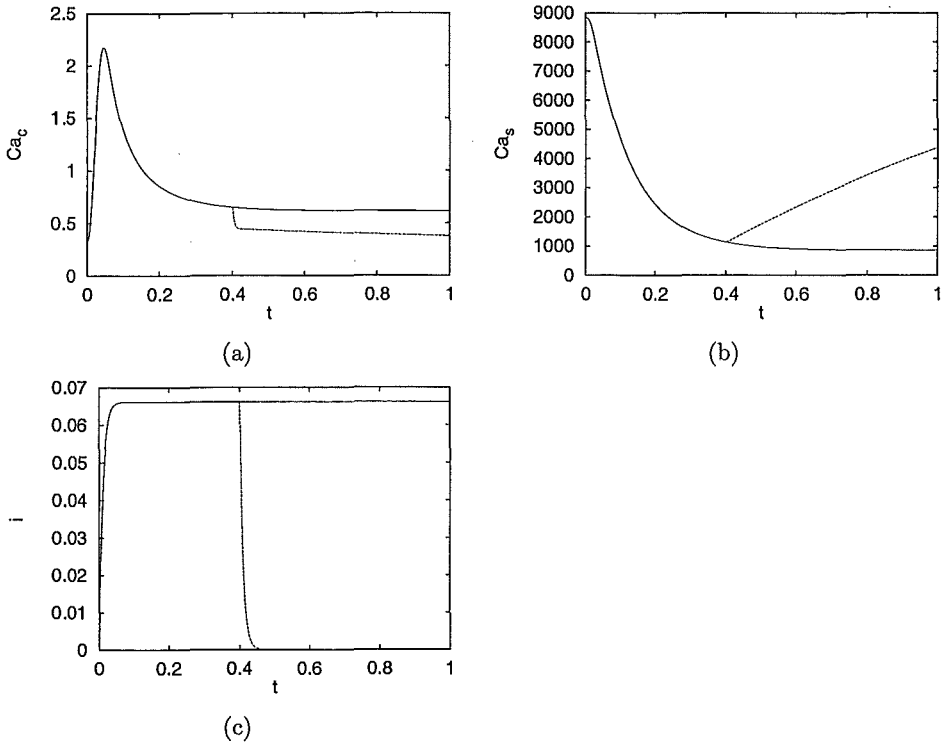

Figure 5: Graph of intracellular concentrations against time in a cell stimulated by a step increase in ATP ($\phi = 0.9$) and shear stress ($\tau_w = 9.2$): (a) Free cytosolic Ca^{2+}. (b) Stored Ca^{2+}. (c) IP_3. The dashed line shows the behaviour after removal of the external ATP and shear stress stimuli at $t = 0.4$: IP_3 rapidly decays to zero, the stores recover towards the resting level and the cytosolic plateau level returns to baseline.

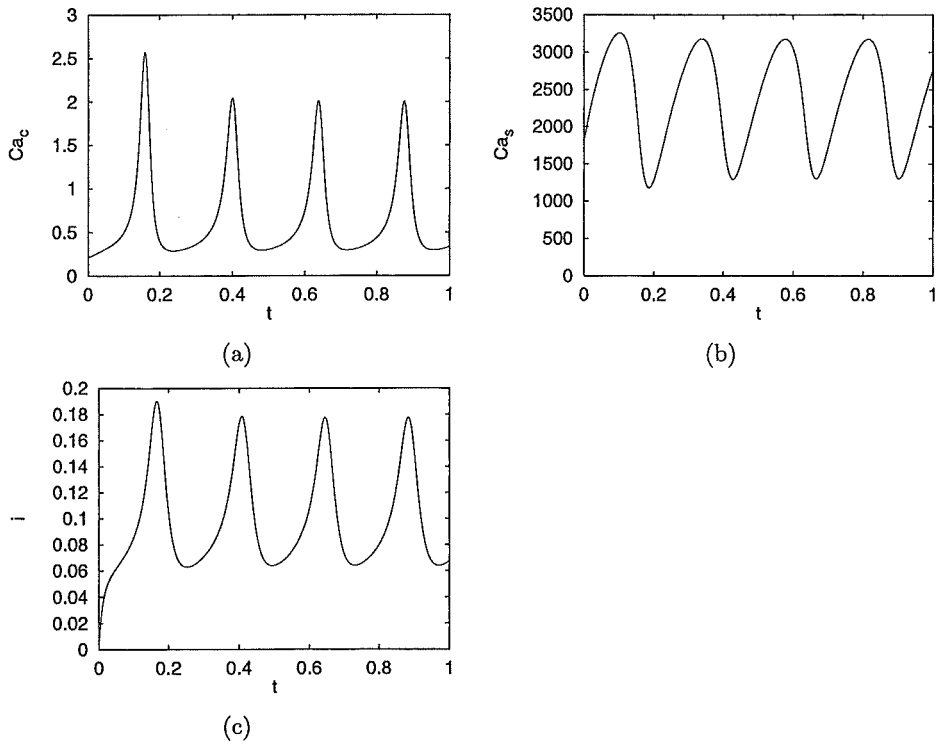

Figure 6: Graph of Ca^{2+} concentrations against time in an ATP-stimulated cell with $k_1 = 35.8$, $k_4 = 7.81 \times 10^4$, $k_5 = 1.6 \times 10^{-4}$ and $K_1 = 1$: (a) Free cytosolic Ca^{2+}. (b) Stored Ca^{2+}. (c) IP_3. The cell undergoes sustained Ca^{2+} oscillations.

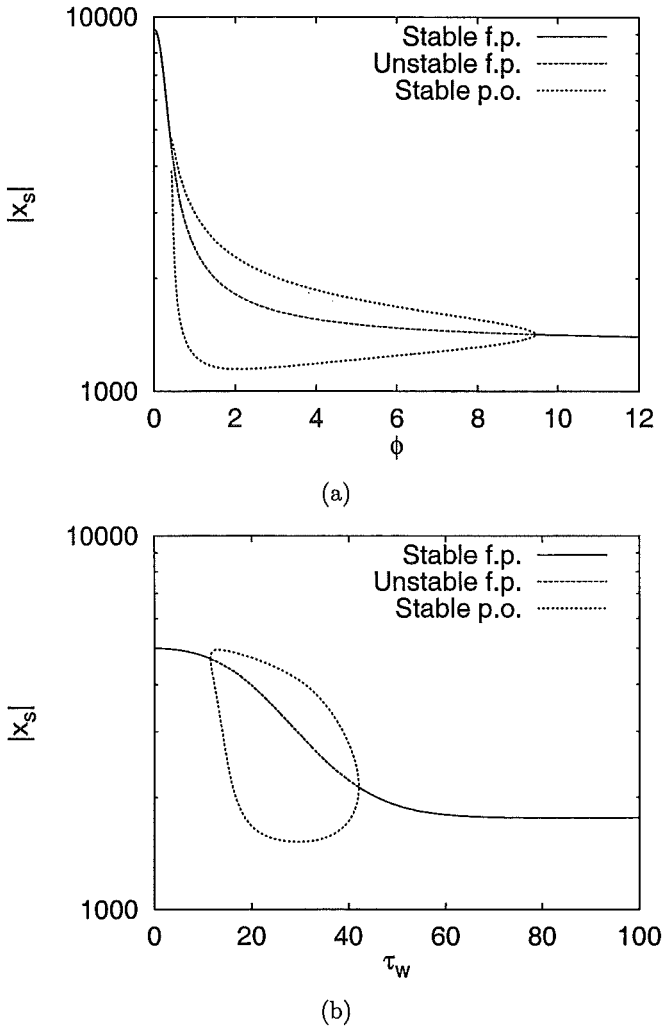

Figure 7: Bifurcation diagrams of the norm of the steady state of the system, $|x_s|$, against (a) ATP concentration, ϕ. (b) Wall shear stress, τ_w. For fixed shear stress, $\tau_w = 9.2$, the system has an unstable fixed point and a stable periodic orbit for $0.42 < \phi < 9.38$, and has a stable fixed point for ϕ outside this range. Similarly, for fixed ATP, $\phi = 0.4$, the system has an unstable fixed point and a stable periodic orbit for $11.5 < \tau_w < 42.1$, and has a stable fixed point for τ_w outside this range. Abbreviations: fixed point (f.p.); periodic orbit (p.o.).

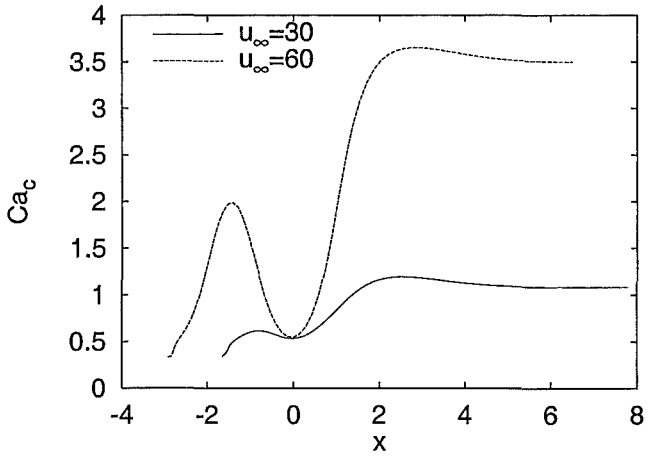

Figure 8: Graph of the stable steady value of Ca_c against x for two different flow velocities, u_∞. The origin ($x = 0$) is chosen to be at the reattachment point. Ca_c is lowest in the recirculation zone due to low wall shear stress and low ATP concentration.

Figure 9 shows a similar graph with simulations run using the oscillatory parameter regime found in section 4 (i.e. $k_1 = 35.8$, $k_4 = 7.81 \times 10^4$, $k_5 = 1.6 \times 10^{-4}$ and $K_1 = 1$). In line with the bifurcation analysis performed above, sustained Ca^{2+} oscillations occur in regions of the endothelium ($-0.9 < x < -0.8$ and $0.4 < x$) for which the combined (shear stress and ATP) external stimulus is above a threshold value. In regions ($x < -0.9$ and $-0.8 < x < 0.4$) where the combined stimulus is below threshold (primarily in and near to the recirculation zone), there are no oscillations and Ca_c settles to a stable steady state. As in the non-oscillatory case (Figure 8), Ca^{2+} signalling is low in the recirculation zone immediately next to the step, but high further downstream.

6 Discussion

A general mathematical model of chemical species concentration in the bloodstream has been coupled with a mathematical model of calcium signalling in EC. This enables the endothelial response to both biochemical and mechanical stimuli of varying strengths to be evaluated. This response is closely linked to the onset of intimal hyperplasia and, as such, this study represents the first step in addressing the central question of why atherosclerosis occurs more frequently in areas of disturbed flow and low wall shear stress.

The mass transport model presented in section 2 calculates chemical concentrations in an arbitrary vessel geometry with known shear stress profile, via an analytical similarity solution. This has been used with a realistic "downstream" input condition to determine the effect of a change in the vessel geometry (namely a backward-facing step) on the concentration of the key endothelial signalling factor, ATP, at the endothelium.

Endothelial Ca^{2+} dynamics have been modelled, in section 3, using ordinary differential equations, which consider average concentrations for the entire cell; spatial variation within a cell is effectively ignored. It is worth noting that intracellular variations and spatial Ca^{2+} interactions, such as Ca^{2+} waves, have been observed experimentally (Sanderson *et al.*, 1990). However, we believe that the approach taken here is justified because we are interested mainly

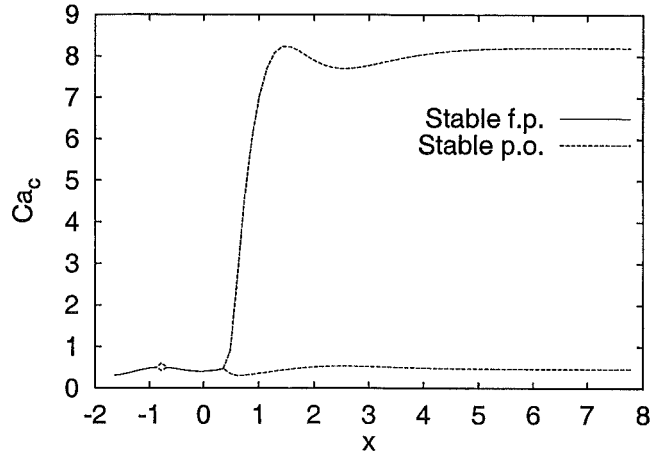

Figure 9: Graph of the stable steady value of Ca_c against x with $u_\infty = 30$, $k_1 = 35.8$, $k_4 = 7.81 \times 10^4$, $k_5 = 1.6 \times 10^{-4}$ and $K_1 = 1$. Again Ca_c is lowest in the recirculation zone due to low wall shear stress and low ATP concentration, and the Ca^{2+} concentration is steady (solid line). At higher wall shear stress and ATP concentration, sustained Ca^{2+} oscillations can occur (with maxima and minima represented by the dotted lines). Abbreviations: fixed point (f.p.); periodic orbit (p.o.).

in relatively large scale variations (over 10–100 cell lengths) along the endothelium. A spatial model, based on partial differential equations, may bring a small increase in accuracy, and is a possible problem for future work, but would not compensate for the large increase in model complexity at this stage.

The Ca^{2+} model has shown quantitative agreement with empirical data, and is capable of reproducing both transient peaks in cytosolic Ca^{2+} concentration and sustained Ca^{2+} oscillations, depending on parameter values used. Specifically, oscillations are associated with: a high rate of IP_3 production by activated surface receptors; high rates of Ca^{2+} exchange between the cytosol and internal stores; and co-operative generation of IP_3 by free cytosolic Ca^{2+} (i.e. positive feedback). Model analysis indicates that, as the external stimulus, changes, oscillations will begin at small amplitude and gradually increase; there is no sudden onset of large-amplitude oscillations.

The results of integrating the two models (section 5) demonstrate that low cytosolic Ca^{2+} concentrations are found in EC in contact with the recirculation zone, near the backward-facing step. This is because of the low wall shear stress and ATP concentration in this area. The downstream length of the recirculation zone (and corresponding low Ca^{2+} zone) varies with the flow velocity, but for physiological Reynolds number flow of $Re \simeq 20$, and a step height of $h = 250$ μm, is approximately 500 μm. In regions of high wall shear stress, where the EC are longitudinally aligned in the direction of flow, this would correspond to roughly 5 cell lengths. In low shear stress regions, however, the EC are poorly aligned and there will likely be several tens of cells in the low Ca^{2+} zone. Therefore, the result is significant in that reduced Ca^{2+} levels are not just found in a very small number of EC, but occur over a substantial length of the endothelium.

It is known that one of the consequences of Ca^{2+} signalling in EC is activation of eNOS and subsequent synthesis of NO (Lin *et al.*, 2000). NO inhibits platelet aggregation and adhesion to the endothelium and induces relaxation and non-proliferation of sub-endothelial SMC

(Malek *et al.*, 1999; Shaul, 2003), and is thus a key inhibitor of IH (Traub and Berk, 1998). The model results thus suggest that the correlation of IH with low wall shear stress may be at least partly explained by reduced IP_3 and Ca^{2+} signalling in EC, leading to reduced synthesis of NO. Although this is a tempting conclusion, it is not the complete picture and there are many other factors involved that we have, for the sake of simplicity, ignored. Atherogenesis is not governed simply by intracellular endothelial Ca^{2+} concentrations, but by a complex balance between a wide variety of positive and negative regulatory factors. Endothelial Ca^{2+} signalling in particular is implicated in a range of cellular functions, some of which are atheroprotective (such as NO synthesis), whilst others are associated with a pro-atherogenic phenotype (such as cell proliferation and secretion of growth factors and adhesion molecules) (Libby *et al.*, 1997; Davies, 2000). Thus the net effect of Ca^{2+} signalling on the initiation of atherosclerosis is unknown and, in the light of the results of this study, we hypothesis that low intracellular Ca^{2+} concentrations in the endothelium are associated with atherogenesis.

At present, the model only simulates steady flow conditions. An interesting model extension will be to extend to time-dependent flow, simulating a realistic pulsatile cardiac cycle. The effect of pulsatile flow on ATP concentrations was considered by John and Barakat (2001) in a parallel plate setup and was found to have a relatively minor effect. In addition, because the timescale of flow variability is fast (approximately 1 flow cycle per second) compared to the timescale for Ca^{2+} dynamics, the effect of flow pulsatility on endothelial signalling may be negligible in comparison with spatial variation of stimuli. Nevertheless, it remains important to test the effects of pulsatile flow in vessel geometries other than simple parallel plate, as it may be a contributing factor to atherogenesis in regions of low time-averaged shear stress (where flow reversal will occur during each cycle).

An important model extension will be to include the downstream effects of Ca^{2+} signalling on secretion of signalling molecules such as ATP and vasoactive molecules such as NO, endothelin and angiotensin. Also, explicitly including endothelial permeability as a model variable would allow the process of plaque formation itself, via transmission of LDLs across the endothelium and the aggregation and proliferation of cells in the intima, to be investigated directly. These additions to the model will allow the hypothesis that low endothelial Ca^{2+} is pro-atherogenic to be investigated in greater detail and will help to elucidate the mechanisms involved in the interaction between the endothelium and arterial wall. Synthetic activity by EC will be coupled to the mass transport model via production functions, $S_i(x)$, for each chemical species, creating a potential feedback loop.

We believe that the model presented captures the key behaviour and that this study is an important step towards understanding the link between haemodynamic conditions, endothelial signalling and atherosclerosis. It is now important to develop and refine the model in close conjunction with experimental data on the Ca^{2+} response of EC in different biochemical and mechanical environments. This will help to ascertain accurate parameter values for the model, to quantitatively test model predictions and to ensure that the model is biologically realistic. Conversely, the model may be used to rapidly simulate a range of potential experimental scenarios, and thus suggest key issues that need to be addressed empirically.

Appendix

ATP reaction rates. John and Barakat (2001) cited an ATP production rate of $V_m = 0.08$ μM m s^{-1}, with associated Michaelis–Menten constant of $K_m = 475$ μM, and a maximum ATP production rate of $S_0 = 10^{-6}$ μM m s^{-1}. The choice of $\tau_m = 5$ kg m^{-1} s^{-2} means that ATP production is sensitive to wall shear stress in the physiological range 0–5 Pa.

ATP diffusion coefficient. $D = 2.36 \times 10^{-10}$ m^2 s^{-1} is the value quoted by John and

Barakat (2001).

Step height. Again $h = 2.5 \times 10^{-4}$ m is the step height used by John and Barakat (2001).

IP_3 rates. Wiesner *et al.* (1996) took the rate of IP_3 production to be proportional to the cumulative amount of modified receptors, R'_A in the reaction (12). Thus a short impulse of ATP stimulation would lead to sustained IP_3 production and the external concentration of ATP affects only the IP_3 response time and not the final IP_3 concentration. We do not believe this is realistic and take a different point of view by assuming that it is the decomposition step itself that triggers the production of IP_3. The IP_3 production and decay rate constants, $k_1 = 5.46 \times 10^{-3}$ μM s^{-1} and $k_2 = 0.2$ s^{-1}, are chosen to maintain a comparable timescale for IP_3 production, and a comparable steady state concentration of IP_3, at physiological levels of ATP. These values are similar to those cited by Mahama and Linderman (1994).

Ca^{2+} exchange rates. Meyer and Stryer (1988) determined the functional forms used for Ca^{2+} release and resequestration and estimated the respective rate constants as $k_3 = 6.64$ s^{-1} and $k_4 = 5$ μM s^{-1} and the associated Michaelis–Menten constants as $K_2 = 0.2$ μM and $K_3 = 0.15$ μM. The Ca^{2+} leak rate was estimated by Wiesner *et al.* (1996) to be $k_5 = 10^{-7}$ μM^{-1} s^{-1}. Wiesner *et al.* (1996) also quoted a cytosolic to ER volume ratio of $V_r = 3.5$.

Ca^{2+} buffering rates. The rates of buffering and debuffering of Ca^{2+} to proteins in the cytosol were measured by Bayley *et al.* (1984) to be $k_6 = 100$ μM^{-1} s^{-1} and $k_7 = 300$ s^{-1} respectively. The total concentration of Ca^{2+} binding sites in the cytosol was estimated by Jafri *et al.* (1992) to be $B_T = 120$ μM.

Ca^{2+} efflux rate. Valant *et al.* (1992) fitted the functional form for Ca^{2+} efflux to be a sum of Hill functions. We approximated this by a single Michaelis–Menten term, with the constants, $k_8 = 24.7$ μM s^{-1} and $K_4 = 0.32$ μM, chosen to approximate the Valant *et al.* (1992) curve over a physiological range of Ca^{2+} concentrations.

CCE rate. Wiesner *et al.* (1996) did not include CCE in their base model, but tested the effects of CCE for values in the range $0 \leq k_{\mathrm{CCE}} \leq 10^{-5}$ μM^{-1} s^{-1}. We took $k_{\mathrm{CCE}} = 8 \times 10^{-7}$ μM^{-1} s^{-1}, which gives a realistic plateau concentration of free cytosolic Ca^{2+} under conditions of prolonged ATP stimulation, but also examined the effects of changing k_{CCE}.

Shear-dependent Ca^{2+} influx. The values of f_e, ϵ, N, l and δ in the energy density function, $W(\tau_w)$, were taken from Wiesner *et al.* (1997). Wiesner *et al.* (1997) estimated the open fraction of shear-sensitive plasma membrane Ca^{2+} channels under no-load conditions to be 25% (i.e. $\alpha = 3$). However, for the given Ca^{2+} efflux rates, this can result, at high shear stress, in non-physioloigcal cytosolic Ca^{2+} concentrations. We therefore took the no-load open fraction of Ca^{2+} channels to be 33% (i.e. $\alpha = 2$), which means that the Ca^{2+} efflux mechanism can maintain the cytosolic Ca^{2+} concentration at physiological levels. The value of q_{max} was taken such that, under resting conditions (i.e. $W(\tau_w) = 0$), cellular homeostasis is maintained (i.e. Ca^{2+} influx is balanced by efflux). The value of $T_e = 310$ K is body temperature.

Ca^{2+} concentrations. The resting free cytosolic Ca^{2+} concentration of $Ca_0 = 0.1$ μM and the external Ca^{2+} concentration of $Ca_{\mathrm{ex}} = 1500$ μM are the values used by Wiesner *et al.* (1996). The resting stored Ca^{2+} concentration of $Ca_{s,0} = 2828$ μM is chosen to satisfy cellular homeostasis under resting conditions (i.e. net exchange of Ca^{2+} between the ER and the cytosol is zero).

CICR and Ca^{2+}-sensitive IP_3 production. Few data are available on the positive feedback mechanisms of CICR and Ca^{2+}-sensitive IP_3 production, so we have initially taken $K_{\mathrm{CICR}} = K_1 = 0$, which means that there is no positive feedback on Ca^{2+} release from stores. However, the effects of including these mechanisms in the model are examined.

References

Alberts, B., Bray, D., Lewis, J., Raff, M., Roberts, K., and Watson, J. D. (1994). *The molecular biology of the cell* (3rd ed.). New York: Garland.

Bayley, P., Ahlstrom, P., Martin, S. R., and Forsen, S. (1984). The kinetics of calcium binding to calmodulin: quin 2 and ANS stopped-flow fluorescence studies. *Biochem. Biophys. Res. Comm.* **120**, 185–91.

David, T. (2003). Wall shear stress modulaiton of ATP/ADP concentration at the endothelium. *Ann. Biomed. Eng.* **31**, 1231–7.

David, T., Thomas, S., and Walker, P. G. (2001). Platelet deposition in stagnation point flow: an analytical and computational solution. *Med. Eng. and Phys.* **23**, 299–312.

Davies, P. F. (2000). Spatial haemodynamics, the endothelium and focal atherogenesis: a cell cycle link? *Circ. Res.* **2000**, 114–6.

Dull, R. O. and Davies, P. F. (1991). Flow modulation of agonist (ATP)-response (Ca^{2+}) coupling in vascular endothelial cells. *Am. J. Physiol.* **261**, H149–54.

Geiger, R. V., Berk, B. C., Alexander, R. W., and Nerem, R. B. (1992). Flow-induced calcium transients in single endothelial cells: spatial and temporal analysis. *Am. J. Physiol.* **262**, C1411–7.

Gimbrone, M. A. (1999). Vascular endothelium, haemondynamic forces and atherogenesis. *Am. J. Path.* **155**, 1–5.

Goldbeter, A., Dupont, G., and Berridge, M. J. (1990). Minimal model for signal-induced Ca^{2+} oscillations and for their frequency encoding through protein phosphorylation. *Proc. Natl. Acad. Sci. USA* **87**, 1461–5.

Jaffe, E. A., Grulich, J., Weksler, B. B., Hampel, G., and Watanabe, K. (1987). Correlation between thrombin-induced prostacyclin production and inositol trisphosphate and cytosolic free calcium levels in cultured human endothelial cells. *J. Biol. Chem.* **262**, 8557–65.

Jafri, M. S., Vajda, S., Pasik, P., and Gillo, B. (1992). A membrane model for cytosolic calcium oscillations. A study using Xenopus oocytes. *Biophys. J.* **63**, 235–46.

Jessup, W., Kritharides, L., and Stocker, R. (2004). Lipid oxidation in atherogenesis: an overview. *Biochem. Soc. Trans.* **32**, 134–8.

John, K. and Barakat, A. I. (2001). Modulation of ATP/ADP concentration at the endothelial surface by shear stress: effect of flow-induced ATP release. *Ann. Biomed. Eng.* **29**, 740–51.

Kwan, H. Y., Huang, Y., and Yao, X. (2000). Store-operated calcium entry in vascular endothelial cells is inhibited by cGMP via a protein kinase G-dependent mechanism. *J. Biol. Chem.* **275**, 6758–63.

Kwan, H. Y., Leung, P. C., Huang, Y., and Yao, X. (2003). Depletion of intracellular Ca^{2+} stores sensitises the flow-induced Ca^{2+} influx in rat endothelial cells. *Circ. Res.* **92**, 286–92.

Libby, P. (2003). Vascular biology of atherosclerosis: overview and state of the art. *Am. J. Cardiol.* **91**, 3A–6A.

Libby, P., Sukhova, G., Lee, R. T., and Liao, J. K. (1997). Molecular biology of atherosclerosis. *Intl. J. Cardiol.* **62**, S23–9.

Lin, S., Fagan, K. A., Li, K. X., Shaul, P. W., Cooper, D. M. F., and Rodman, D. M. (2000). Sustained endothelial nitric-oxide synthase activation requires capacitative Ca^{2+} entry. *J. Biol. Chem.* **275**, 17979–85.

Mahama, P. A. and Linderman, J. L. (1994). Calcium signalling in individual BC_3H1 cells: speed of calcium mobilisation and heterogeneity. *Biotechnol. Prog.* **10**, 45–54.

Malek, A. M., Alper, S. L., and Izumo, S. (1999). Haemodynamic shear stress and its role in atherosclerosis. *J. Am. Med. Assoc.* **282**, 2035–42.

Meyer, T. and Stryer, L. (1988). Molecular model for receptor-stimulated calcium spiking. *Proc. Natl. Acad. Sci. USA* **85**, 5051–5.

Milner, P., Kirkpatrick, K. A., Ralevic, V., Toothill, V., Pearson, J., and Burnstock, G. (1990). Endothelial cell cultures from human umbilical vein release ATP, substance P and acetylcholine in response to increased flow. *Proc. R. Soc. Lond. B* **241**, 245–8.

Murray, J. D. (1993). *Mathematical biology* (2nd ed.). Berlin: Springer-Verlag.

Putney, J. W., Broad, L. M., Braun, F. J., Lievremont, J. P., and Bird, G. J. (2001). Mechanisms of capacitative calcium entry. *J. Cell Sci.* **114**, 2223–9.

Sanderson, M. J., Charles, A. C., and Dirksen, E. R. (1990). Mechanical stimulation and intercellular communication increases intracellular Ca^{2+} in epithelial cells. *Cell Regul.* **1**, 585–96.

Schachter, M. (1997). The pathogenesis of atherosclerosis. *Intl. J. Cardiol.* **62**, S3–7.

Schilling, W. P. and Elliott, S. J. (1992). Ca^{2+} signalling mechanisms of vascular endothelial cells and their role in oxidant-induced endothelial cell dysfunction. *Am. J. Physiol.* **262**, H1617–30.

Shaul, P. W. (2003). Endothelial nitric oxide synthase, caveolae and the development of atherosclerosis. *J. Physiol.* **547**, 21–33.

Shen, J., Luscinskas, F. W., Connolly, A., Dewey, C. F., and Gimbrone, M. A. (1992). Fluid shear stress modulates cytosolic free calcium in vascular endothelial cells. *Am. J. Physiol.* **262**, C384–90.

Tran, Q. K., Ohashi, K., and Watanabe, H. (2000). Calcium signalling in endothelial cells. *Cardiovasc. Res.* **48**, 13–22.

Traub, O. and Berk, B. C. (1998). Laminar shear stress: mechanisms by which endothelial cells transduce an atheroprotective force. *Arterioscler. Thromb. Vasc. Biol.* **18**, 677–85.

Tseng, H., Peterson, T. E., and Berk, B. C. (1995). Fluid shear stress stimulates mitogen-activated protein kinase in endothelial cells. *Circ. Res.* **77**, 869–78.

Valant, P. A., Adjei, P. N., and Haynes, D. H. (1992). Rapid Ca^{2+} extrusion via the Na^+/Ca^{2+} exchanger of the human platelet. *J. Membrane Biol.* **1992**, 63–82.

Watanabe, H., Takahashi, R., Zhang, X., Goto, Y., Hayashi, H., Ando, J., Isshiki, M., Seto, M., Hidaka, H., Niki, I., and Ohno, R. (1998). An essential role of myosin light-chain kinase in the regulation of agonist- and fluid flow-stimulated Ca^{2+} influx in endothelial cells. *FASEB J.* **12**, 341–8.

Wiesner, T. F., Berk, B. C., and Nerem, R. M. (1997). A mathematical model of the cytosolic-free calcium response in endothelial cells to fluid shear stress. *Proc. Natl. Acad. Sci.* **94**, 3726–31.

Wiesner, T. F., Berk, B. C., and Nerem, R. N. (1996). A mathematical model of cytosolic calcium dynamics in human umbilical vein endothelial cells. *Am. J. Physiol.* **270**, C1556–69.

Wood, P. G. and Gillespie, J. I. (1998). Evidence for mitochondrial Ca^{2+}-induced Ca^{2+} release in permeabilised endothelial cells. *Biochem. Biophys. Res. Comms.* **246**, 543–8.

Yamamoto, K., Korenaga, R., Kamiya, A., and Ando, J. (2000). Fluid shear stress activates Ca^{2+} influx into human endothelial cells via P2X4 purinoceptors. *Circ. Res.* **87**, 385–91.

Yamamoto, K., Sokabe, T., Ohura, N., Nakatsuka, H., Kamiya, A., and Ando, J. (2003). Endogenously released ATP mediates shear stress-induced Ca^{2+} influx into pulmonary artery endothelial cells. *Am. J. Physiol.* **285**, H793–803.